Synchrotron studies of carbon surfaces

2001 J. Phys.: Condens. Matter 13 11229

(http://iopscience.iop.org/0953-8984/13/49/309)

INSTITUTE OF PHYSICS PUBLISHING JOURNAL OF PHYSICS: CONDENSED MATTER

J. Phys.: Condens. Matter **13** (2001) 11229–11248 PII: S0953-8984(01)29261-3

Synchrotron studies of carbon surfaces

P A Brühwiler

Department of Physics, Uppsala University, Box 530, SE-751 21 Uppsala, Sweden

E-mail: Paul.Bruhwiler@fysik.uu.se

Received 28 September 2001
Published 10 December 2001
Online at stacks.iop.org/JPhysCM/13/11229

Abstract

I review the use of synchrotron radiation to study the structural and electronic properties of carbon surfaces, including diamond, graphite, nanotubes and C_{60}.

(Some figures in this article are in colour only in the electronic version)

1. Introduction

Carbon is a ubiquitous element in nature and society, with a fascinating variation in its forms and properties. Focussing only on pure and relatively stable forms as I will do here, an extreme variabilty emerges, roughly in order of decreasing symmetry and dimension (see figure 1): the three-dimensional insulator diamond, two-dimensional semimetal graphite, one-dimensional molecular wires and/or semiconductors the nanotubes and zero-dimensional molecular solids the fullerenes. There is also a myriad of other carbon materials one could consider [1]. The concept of a surface for these materials is somewhat dependent on one's point of view—the C_{60} molecule itself can be considered a spherical graphite-like surface, and the nanotubes to be rolled-up sheets of graphite. Being a highly anisotropic material, the graphite surface is quite similar to the bulk in many respects. Since these materials all embody low-dimensional character as expected for surfaces, I take the liberty of including them in a discussion of synchrotron studies of carbon surfaces. There will naturally be points in common with, for example, studies of organic molecules and layered materials like transition metal dichalcogenides, but I will make no detailed connections to that work. I shall, on the other hand, make use of compounds which illuminate the low-dimensional nature of the materials when appropriate, such as those with alkali metals.

The organization of this review is as follows: I describe the basic experimental methods employed in the studies which are included. Then I approach the studies material for material, taking structural characterizations first, to emphasize the importance of structural models when interpreting studies of the electronic states; then vibrational properties, when available; and finally, studies of the electronic structure. Finally, I will give a brief summary of the work presented, and a personal view of the outlook for future work in the 'field' of carbon surfaces. This review will due to length restrictions not be exhaustive, but will hopefully give a 'flavour' of what has been and can be accomplished.

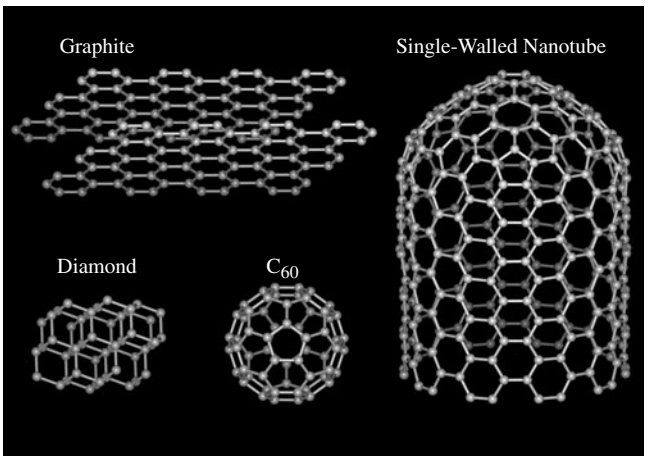

Figure 1. Schematic of the crystalline allotropes of carbon whose surfaces will be taken up in this review.

2. Experimental techniques

X-ray diffraction (XRD) is a tool which needs little introduction. Relevant here is the fact that carbon has a low scattering coefficient due to its relatively low charge density. Thus, in studies of adsorbed fullerenes for which this technique is discussed in this review, the most reliable structural information is gained on the accompanying substrate reconstructions, and not details of the fullerene configurations. The synchrotron provides flexibility in choosing the x-ray wavelength, and high intensity, which are also crucial features for the soft-x-ray techniques described immediately below.

Infrared absorption spectroscopy provides vibrational energies via the peak position of a given vibrational resonance, and electron–phonon coupling parameters via the line profile, as well as adsorbate-induced changes in sample absorption coefficient. Synchrotron radiation offers high intensities which are useful due to the possibility of more accurately studying low frequency modes [2]. This is vital for the studies of adsorbed fullerenes which I discuss below.

Photoelectron spectroscopy (PES, or x-ray photoelectron spectroscopy, XPS) is a fundamental tool in the study of surfaces, because of the intrinsically low mean free path of electrons at sub-kilovolt kinetic energies [3]. Since the mean free path is a function of the kinetic energy, with a typical minimum of about 2–5 Å for energies in the range of 50 eV, it is possible to emphasize surface or bulk features by appropriate choices of the photon energy. Binding energy shifts of core levels give structural information, as well as information on screening effects [4], whereas the valence electronic states are more or less directly accessible using PES. Atomic, molecular and solid state cross section effects can also come into play in determining the energy- and angle-dependences of the spectra, which are particularly simple in the case of the 1s level, but in general much more complex for excitations of valence levels to moderate kinetic energies. Angle-resolved PES is capable of delivering quite detailed information on the energy–momentum relationships for the valence electrons in favourable cases [5]. Resonant PES (RPES), which can be considered as a decay channel of x-ray absorption [6, 7], is useful, for example, for studying the local atomic character of the valence levels. The broad applicability of the various forms of electron spectroscopy is reflected in the number of examples taken up here.

Soft-x-ray absorption spectroscopy (XAS) is a popular means of studying the frontier unoccupied energy levels of carbon-containing materials, since it can often be measured *in situ*

on a sample already being studied with PES/XPS, making all states around E_F available. Since it is generally the C 1s level which is excited, the dipole selection rule combined with the highly localized distribution of the 1s wavefunction result in spectra which characterize the local p-like density of states at carbon sites for which the excitation energy is appropriate [8]. It is important to take into account the strong perturbation which a core hole entails for the electronic states, but this is increasingly feasible with modern computational power, as is illustrated in examples given below. XAS can also give qualitative, and even quantitative, information on bondlengths, and has a strong symmetry selectivity which is especially easy to interpret for 1s excitations [8]. This technique, like PES/XPS, has been used on all the carbon materials discussed in this review. Since electron yield (Auger primary and/or secondary electrons) are used for detection, XAS can be employed with a variable surface sensitivity to give access to the surface-specific core excitations. RPES can be used to analyse the XAS spectra for cases of more heterogeneous samples, and hence more complex spectra, since the local electronic structure at a particular atomic site often leads to significant differences in XAS and its decay channels. A detailed discussion of the relative energy calibration of XAS and PES/XPS has recently been given in a separate review [7]. On the practical side, the challenge in studying XAS of carbon materials is that the beamline optics can contain C and/or Cr, both of which contribute to the effective transmission of a soft-x-ray beamline in the relevant energy range, introducing and/or suppressing structures in a spectrum [9].

A technique intimately connected to XAS is soft-x-ray emission spectroscopy (XES) [10] and the related process resonant inelastic x-ray scattering [11–13], so denoted because it is a coherent photon-in–photon-out process. These techniques are complementary to PES and ARPES, respectively, and are normally bulk-sensitive due to the relatively long mean free path of photons in matter. For coherent scattering, energy and momentum conservation rules may be applied, which connect the available final (valence) hole states to the chosen (conduction) electron state. The electron state, in turn, is selected by tuning the excitation energy as in XAS. For cases such as graphite, nanotubes and fullerenes, the information available with XES and RIXS is to a good approximation that of the relevant 'carbon surface' even for thick films, due to the weak interactions among the subunits of the material (layer, tube and molecule, respectively).

3. Diamond

Diamond has a cubic structure in which each atom is surrounded by four others arranged at the vertices of a tetrahedron [1], which can be thought of as two identical interspersed fcc lattices (see figure1). It is technologically interesting for among other reasons its insulating nature, hardness, low friction and high thermal conductivity, which are attractive in, for example, electronics [14] and surface coatings [15] applications. Of the three low-index faces of diamond, the (111) and (100) are relatively well studied, whereas the (110) is still quite difficult to prepare [16]. The hydrogenated (100) and (111) surfaces of diamond are known to be stable in air, and can be cleaned by heating in vacuum. A challenge for the study of single-crystal diamond surfaces is that natural crystals are generally used, and this appears to constitute a barrier in efforts to obtain agreement among different studies [17, 18].

A history of the study of atomically clean and hydrogenated diamond surfaces is given in [14]. An early synchrotron study established the existence of a *negative* electron affinity of the hydrogenated (111)(1 × 1) surface [19], at the time known only for this semiconductor. While the electron affinity itself has become a significant topic of research for diamond surfaces, it has the side benefit that it induces a peak in PES data which can be used to calibrate the spectra relative to the diamond bandstructure [20], and thus also a calibration on XAS [7].

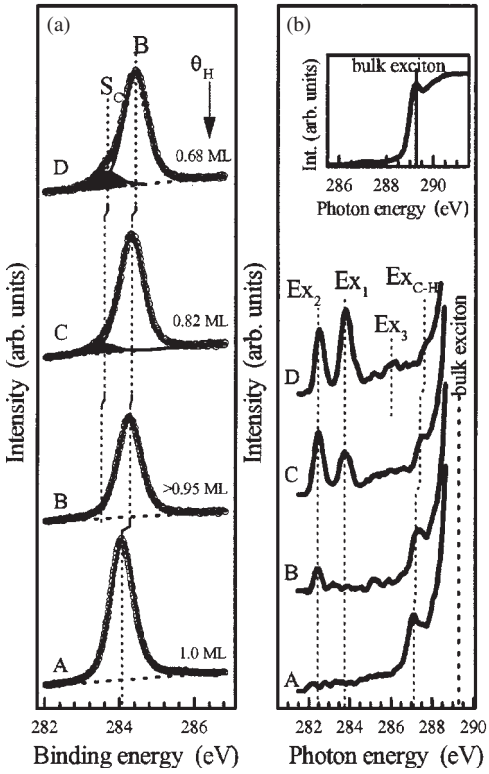

Figure 2. (a) C 1s XPS of the (100) diamond surface as a function of H-coverage, showing that the 1s binding energy of hydrogenated C atoms is quite similar to that of the bulk. (b) Corresponding XAS spectra: Ex_1 and Ex_3 are assigned to C atoms with π-bonded dangling bonds with excitonic and band-resonance character, respectively [21, 22], $Ex_{C–H}$ to a surface state associated with atoms bound to hydrogen [21, 23], and Ex_2 to isolated dangling bonds on the partially hydrogenated surface [22].

This was used in an early study of the structure of the diamond (111) surface using XPS [24]. Those workers observed surface C 1s shifts for the clean and fluorinated surfaces, but virtually none for a hydrogenated surface. From the surface core level intensity, they concluded that the clean surface (2×1) reconstruction involves only a single layer of C atoms, in basic agreement with a calculation [25] which has since received much additional support in many other studies, although details of the structure of the surface layer remain under debate [26]. A very low value of the electron mean free path of 2.1 Å for kinetic energies near 40 eV also emerged from this study, which was attributed speculatively to the very high atomic density of diamond. More recently, the degree of hydrogenation was monitored using the C 1s shift of the clean surface [22] as a function of hydrogen exposure of the clean surface, as well as heating or synchrotron irradiation of hydrogenated surfaces.

In the first study of a diamond surface using C 1s XAS, it was concluded that both surface excitons and delocalized π^* states could be identified [27] at the (111) surface. Later work using more sophisticated sample preparation techniques reproduced those results [21], although all resonances were identified as relatively localized (Frenkel, rather than Wannier, excitons, although another point of view has been advanced for the bulk case [28]). For the clean (001) surface [21, 22] two surface resonances were observed, which were assigned to π-bonded dangling bonds (see figure 2). Hydrogenated surfaces have also received attention recently. A 'C–H exciton' was first identified on the (100) surface, which used H-ion detection to improve the surface sensitivity of XAS [23, 29]. Soon after it was concluded that hydrogenated (100) and (111) surfaces both exhibit this surface core exciton characteristic of H-termination [21] at about 287.5 eV. The most recent work showed narrower and more numerous surface 1s resonances [22]. One resonance emerges only for partial hydrogen coverages, leading to its

assignment in terms of single dangling bonds. C 1s XAS is thus shown to be a sensitive probe of the surface electronic structure, and indirectly the atomic structure as well. Theoretical analysis of the observed structures would also be invaluable, and appears to be feasible, given the success of recent studies of excitonic effects in *bulk* diamond 1s XAS [30, 31].

4. Graphite

Graphite has a layered hexagonal structure; as seen in figure 1, it can be considered to consist of 'graphene' sheets, for which there are two atoms per two-dimensional unit cell. The sheets are then arranged such that one of the atoms in each unit cell of a given sheet is aligned with an atom on each of the neighbouring sheets, whereas the other is aligned with the centre of a hexagon, breaking the equivalence of these atoms in two dimensions [32]. The (0001) surface of graphite typically studied is thus a slightly modified graphene sheet, and because of the weak interlayer interaction [32, 33] the electronic structure of solid graphite differs only weakly from that of graphene. This makes the (0001) surface of this system an ideal test-case for two-dimensional effects, as well as for ARPES and XAS, as will become apparent. Since the structure of the (0001) surface is not usually in question, I merely point out that many studies are performed on so-called highly oriented pyrolytic graphite (HOPG), which is characterized by a degree of disorder in the relative orientation of neighbouring graphene layers [1] compared to single-crystal graphite. More recently, single-crystal quality graphite has been produced and characterized for surface studies by annealing 6H–SiC(0001) [34]. The graphite surface is very forgiving with regard to vacuum requirements, as well, since it is quite unreactive and can stay clean for days in UHV.

The electronic structure of graphene can be understood in terms of strong σ bonds directed from atom to atom within the plane, and weak π bonds above and below the plane [33, 35, 36]. This is reflected in a large gap between bonding and anti-bonding σ bands, within which the bonding and anti-bonding π-bands reside. The bands are roughly centred around E_F, which also locates a minimum in the density-of-states (DOS), making graphene a zero-gap semiconductor [32], which becomes a semimetal in the three-dimensional system.

4.1. Graphite C 1s PES

Since core-level PES often gives structural information, it is natural to consider the C 1s spectrum first, although much of the interest in the spectrum is focussed on the electron correlation effects which contribute to the asymmetric lineshape [37–41]. The asymmetry is typically characterized by a parameter α. This and the lifetime and vibrational widths of a core line, γ and Γ_G, respectively, can be expected to be sensitive to 'extrinsic' properties such as defects, as well as differences between surface and subsurface layers, making these parameters an interesting measure of data quality and interpretation.

In the first study aimed at this issue based on data taken with a rotating anode x-ray source [37], and thus a resolution of several tenths of an eV, $\alpha = 0.14$ was derived, with γ left unspecified. This value of α is similar to what has been found for free electron metals [42]. Since α is related to the screening charge associated with the core hole, which was assumed at the time to be relatively low for a semimetal such as graphite, a novel explanation in terms of a C 1s exciton in the unoccupied DOS [43] was invoked [37]. The advent of high-resolution soft x-ray beamlines [44] enabled a fresh look at this problem. It was concluded in the first such study with a resolution of 125 meV that the handling of (so-called extrinsic) electron scattering effects on the lineshape was crucial to obtaining a reliable value of α [38]; the 'best value' was then found to be 0.065 ± 0.015, whereas the value of $\gamma = 210 \pm 10$ meV derived

was unexpectedly high, leading to speculations of novel screening processes in solid carbon materials. At the same time, the lack of an observable temperature dependence was interpreted as due to a very weak vibrational coupling to a 1s hole in graphite.

A later study using a resolution as low as 80 meV aimed at identifying a surface core level shift found no such shift, but lowered the highest reasonable value of γ to 165 ± 15 meV [40], and of α to 0.056. The vibrational broadening Γ_G could not be derived, but it was concluded that the still relatively high value of γ was most likely due to a non-Gaussian vibrational profile, and thus represented a quite high upper limit. Finally, the most recent results which were taken at 100 K and a resolution of about 50 meV could identify a surface core level shift of 120 meV by employing different photon energies to make use of final-state-induced suppression of the bulk contribution to the spectra [41]. The value $\alpha = 0.048 \pm 0.006$ and the upper limit of $\gamma \leqslant 160$ meV found there is similar to the results of [40]. $\gamma \leqslant 160$ meV is still relatively large compared to small molecules, which was attributed tentatively to the inability to resolve the contributions from the two inequivalent carbon sites in a given graphene layer (surface or bulk), as well as possible smaller layer-dependent shifts for the bulk layers. The low value of $\Gamma_G \sim 60$ meV found, combined with a lack of vibrational loss structure, was concluded to imply a low coupling to vibrations for graphite. To summarize the studies of C 1s PES of pristine graphite, recent higher resolution studies have enabled the identification of surface and bulk contributions to the spectra, but there remain open questions regarding the core hole lifetime and vibrational coupling, which may hinge on the inability to resolve the two carbon sites expected on symmetry grounds. It seems clear that the vibrational coupling in the 1s XPS must be $\leqslant$0.1 eV. Some of these issues are reflected in the electronic structure as well.

4.2. Graphite ARPES

For crystalline solids, the technique of choice to elucidate the electronic structure is angle-resolved photoelectron spectroscopy. As a virtually two-dimensional solid, graphite has long played the role of prototype and testing ground for ARPES [45]. Synchrotron studies of this material brought with them the ability to, for example, easily vary the photon energy to optimize the cross sections of the different bands or avoid unwanted final state effects [36, 46, 47], as well as to enhance the ability to fully explore the Brillouin zone(s) [35, 36, 48, 49].

The six-fold symmetry of graphene and its electronic structure is readily apparent in figure 3, which contains images of the electron distribution at a given kinetic energy as a function of emitted angle, and thus a function of momentum $k_\parallel$ parallel to the surface. Only on closer examination does the symmetry-breaking effect (within the two-atom unit cell of graphene) of the AB-stacking in graphite become apparent as a three-fold symmetry (see, e.g., figures 3(a), (d), (h)). Also visible is the semimetallic nature of graphite, seen here as the 'tails' of the Fermi surface (see, e.g., [1]) at the vertices of the Brillouin zone near the periphery of the image in figure 3(a). The detailed dispersions of the bands measured using ARPES along high-symmetry directions were found to agree quite well with calculations [36, 48]. So far no published study has to my knowledge shown the fine splitting of the graphene bands expected theoretically due to the interlayer interaction [36].

Some of the more recent ARPES of graphite have once again served to refine our understanding of fundamental electron physics. For instance, the value of the bandwidth, which reflects electron–electron correlations, was reassessed using a more efficient two-dimensional electron detector. The experimentally determined value of 22.0 eV is in excellent agreement with the quasiparticle estimate of 21.8 eV [49]. This expansion of about 11% over the one-electron width is reminiscent of insulators, which have similar expansions, and distinct from free electron metals, which show a band-narrowing of similar magnitude [50].

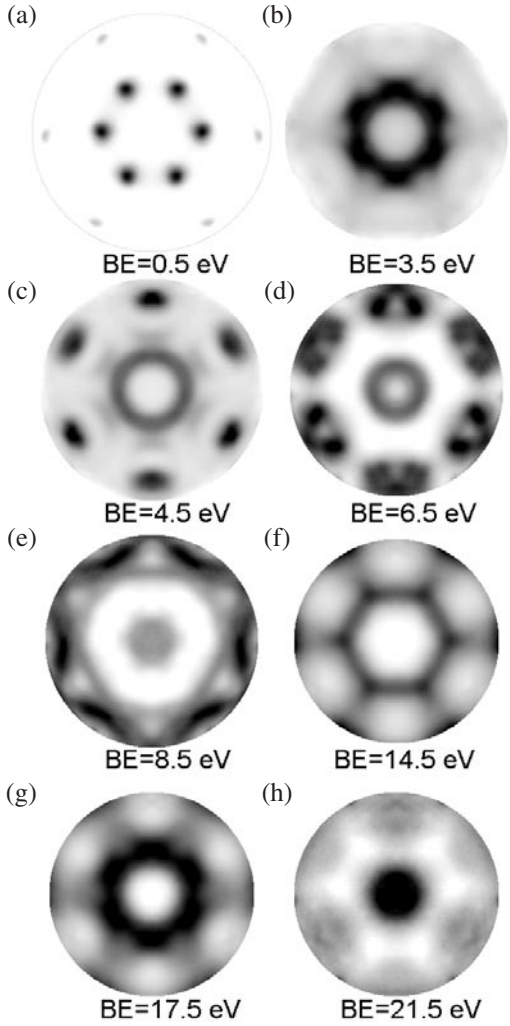

Figure 3. PES intensity as a function of $k_{\parallel}$, otherwise known as photoelectron momentum distribution images, at the indicated binding energies, obtained using a two-dimensional detector [49].

The same detection approach was used to investigate intensity distributions from Brillouin zone to Brillouin zone in ARPES. It was shown experimentally and theoretically that the intensities of the same bands vary as a function of where in k-space they are observed, due for graphite to the fact that there are two atoms per unit cell producing 'initial state interferences' [35].

Another fundamental effect on ARPES intensities recently explored is that of dichroism [51]. Using circularly polarized light, it is possible to arrange an experiment in which the polarization carries over into a 'handedness' in the experimental geometry. This constitutes an asymmetry which is reflected in the angular dependence of the intensity of ARPES excited with left- versus right-handed circularly polarized light. The two-dimensional nature of graphite/graphene allows this to be demonstrated especially clearly.

4.3. XAS/RIXS of graphite

As is apparent in figure 4, 1s XAS of graphite strongly reflects the anisotropy of the physical and electronic structure. Since the p-like DOS is strictly localized within the plane or perpendicular

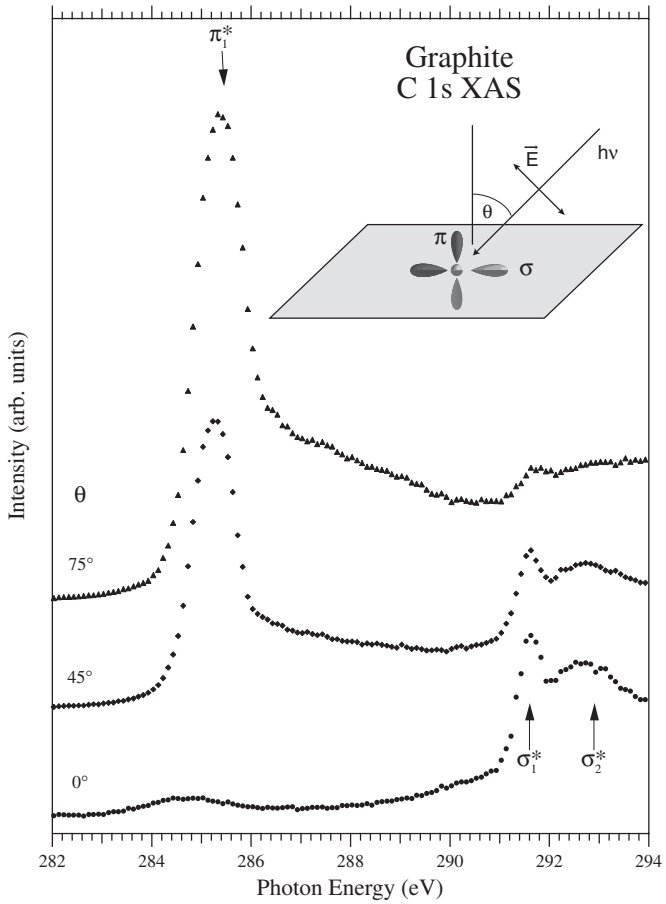

Figure 4. Angle-dependent C 1s XAS data for graphite (HOPG), acquired at a photon resolution of 0.13 eV [52]. Also indicated is the geometrical origin of the observed incidence-angle dependence, since the spectral contributions of π^* and σ^* character scale as the projection squared of the polarization vector perpendicular to or in the plane, respectively [8].

to the plane, control of the angle of incidence of linearly polarized radiation allows one to determine which states will be excited, π^* or σ^*. Thus the data shown here indicate that the picture of the ground state in which the π states lie in a gap of σ symmetry is reflected in XAS, as well, with states of σ symmetry having their onset at about 291 eV.

The first theoretical study of XAS in graphite pointed out, however, that the core hole potential has strong effects on the observed states, similar to the excitons so well known for semiconductors, and discussed for 1s XAS of diamond. Although this point was challenged by later workers, a study in combination with RPES [52], later corroborated quite well by theory [53], supports the original thesis, which has also been supported by more recent calculations [30, 54]. Essentially, RPES can be used to probe the lifetimes of excited states relative to the lifetime of the core hole [7, 55]. This was used to show that both the strong π^* state and the first σ^* state are quite localized, consistent with a description in terms of excitons. The σ^* state had already been shown to resemble the bulk diamond exciton using RIXS [56], which was now further supported by the RPES and theory results.

The well known π^* resonance, however, appears to represent a stronger challenge to understand; its width is approximately 1 eV, and has often been modelled in terms of an electronic coupling (bandwidth) [30, 43, 54]. On the other hand, supercell calculations which were free from parametrizations of the electronic coupling found a much narrower electronic DOS corresponding to this resonance, which had also been suggested by the RPES data [52]. This led to speculations that vibrational coupling which contributes ∼0.6 eV to the width is responsible for the observed profile [53]. Considering the low level of vibrational coupling speculated to occur for the C 1s XPS (see section 4.1), this may seem excessive, but is in qualitative agreement with results on small aromatic molecules. Compare, for example, the case of ethylene (C_2H_4), with an XPS spectrum that is ∼0.3 eV wide [57], and an XAS spectrum that is ∼0.7 eV wide [58]. For benzene (C_6H_6), the corresponding widths are 0.4 eV [59] and 0.7 eV [60], respectively. While these figures are strongly affected by the contributions of C–H vibrations, RIXS data for the first σ^* resonance of graphite make it clear that strong vibrational effects occur on a longer time scale [56]. Another aspect of the π^* resonance which supports the supercell calculation is the derived spatial extent of about eight bond lengths, which would be much larger for a (almost ten times) larger electronic coupling. Recent STM/STS studies of graphite with H-atoms chemisorbed in on-top sites show a significant perturbation of the electronic structure over a quite similar distance, although more subtle effects occur over larger distances [61]. A conclusive resolution of this point awaits a calculation of the vibrational coupling in graphite core spectra.

A related issue is the observation of strongly energy-dependent RIXS in graphite. The dispersion of peaks in RIXS is due to the energy–momentum relationship for electrons and holes in periodic solids. Essentially, the excess energy input in the XAS step (relative to the threshold energy which is 284.4 eV in graphite [52]) determines, in the final state, which crystal momentum has been selected, and places constraints on which final hole states are allowed ($\Delta k = 0$). Interestingly, the wide-band systems thus far which show the band-dispersion effects of RIXS are comprised of semiconductors and graphite, whereas free electron metals have not been found to display this phenomenon [13, 62]. It was appreciated early on that the coherence required for the conservation rules to hold in RIXS may be disturbed by excitation of vibrations [63], electron–hole pairs, or other excitations such as plasmons [62]. The core-excited (or XAS) state which is the RIXS intermediate state is thus crucial, because its lifetime corresponds to the timescale of the RIXS transition [64]. In this regard, the fact that the conservation rules are observed most clearly in the vicinity of the π^* resonance of graphite is easily related to the excitonic effects characterized in XAS—since the electronic coupling to the rest of the system is quite weak in this energy region judging from the widths of the theoretical peaks in figure 5 [52, 53], the coherence of RIXS is less likely to be disturbed due to a lower influence of electronic excitations, with the possible exception of those arising in the XAS step. This aspect of excitons and coherence in RIXS of wide-band solids appears to be often overlooked [13, 62]. The distortion of the unoccupied states in the intermediate (excitonic) state changes their spatial distribution, and could in principle change the intensities of the observed RIXS transitions relative to a calculation which ignored such changes; however, this does not appear to be the case for graphite [30, 54]. The fact that graphite is unique among wide-band 'metals' suggests that one should look to the lower dimensionality of graphene for an explanation, as this would tend to enhance electronic correlations implicit in the excitonic effects observed in XAS. Indeed, the observed band-widening in the graphite valence PES (see section 4.2) places graphite closer to semiconductors and insulators than to metals [50]. Vibrational coupling may play an important role [63,64] in explaining the significant incoherent fraction of the spectra [65, 66]. The strong effects observed in RIXS suggest that in this case as well graphite will continue to serve as a prototype for future studies.

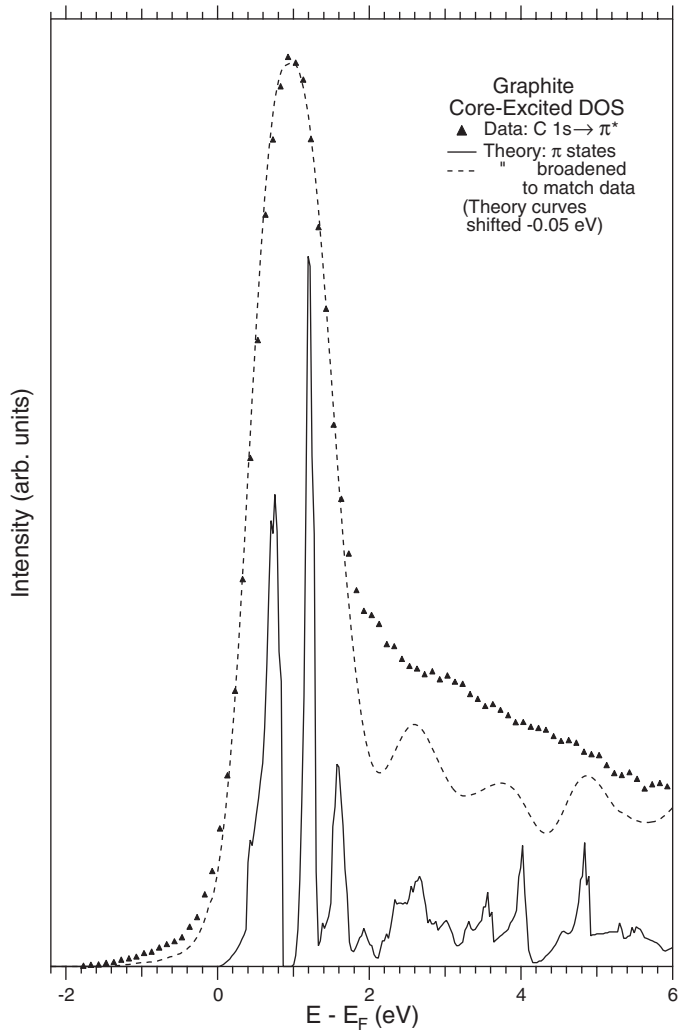

Figure 5. Comparison of theoretical (50-atom supercell, $Z + 1$-DOS) to experimental C 1s XAS data for graphite (HOPG) [53]. The smooth theoretical curve includes a Gaussian broadening of 0.6 eV. Smaller supercells showed similar DOS peak widths in the region of the peak.

4.4. K/graphite

The interactions of alkali metals with the graphite surface constitute perhaps the simplest interaction with which to probe the low-dimensional aspects of surface chemistry, and so is worth a brief mention here. A quite striking behaviour was discovered using electron energy loss spectroscopy when evaporating small quantities of K onto cooled graphite surfaces—a lattice of atoms formed which took up positions of maximal separation, giving evidence of both high mobility and relatively strong inter-K repulsive forces [67]. A high degree of charge transfer could also be estimated from the charge-carrier plasma frequency, which was found to be quite sensitive to charge transfer into the graphite. The overlayer was found to transform to a more or less metallic layer of K as the density increased. These results were corroborated by a synchrotron study of the K 3p, C 1s and valence bands [39]. Notable among the results is

the fact that the valence states and C 1s levels shifted almost rigidly together as a function of the degree of charge transfer to the graphite surface. Though a nearly rigid shift of the valence bands as a function of charge donation is not surprising in a case of simple charge transfer, the fact that the 1s level shifted in a parallel fashion testifies to the uniform ability of graphite to screen a core hole as a function of the DOS at E_F. Also noteworthy was that subsurface layers were found to be virtually unaffected, with the exception of the first subsurface layer.

5. Carbon nanotubes

Carbon nanotubes have much in common with graphite, and indeed can often be thought of to an excellent first approximation as rolled-up graphite, both in terms of their structural [68] and electronic [68, 69] properties. Nanotubes which fit this description have diameters which vary from about 10 to many Å, and lengths which vary from Å to μm. The symmetry of the cylindrical portion of a given nanotube can be specified as 'armchair' or 'zig-zag', which describes the succession of alternating bonds around a cross section of the tube, or chiral. Tubes may be capped or open-ended, and in the former case the cap will typically resemble a fullerene. Nanotubes may be found as isolated individuals, 'ropes' containing a number of tubes, or multiwalled varieties. For the latter cases of multiple individuals, the interlayer spacing is expected to be at a minimum slightly larger than that of the graphene layers in graphite due to the inability to achieve the optimum stacking arrangement [68], which is indeed observed [70–73]. Notably, such information is obtained from an ensemble of ropes in virtually all cases, for which the detailed structures and chiralities of the individual tubes is not fully elucidated, and thus the determined properties are presumed to be average values. Details on smaller ensembles can be obtained by, for example, performing diffraction experiments in a transmission electron microscope (TEM) [74].

With this in mind, it is not surprising that many of the observations of the electronic structure are simply related to those of graphite, modified to take the structural specifics of the given nanotube into account [69, 75], with weak intertube interactions [75]. Interestingly, the quantum confinement in one dimension entailed by the tube diameter leads to van Hove singularities in the DOS both below and above E_F, as well as determining which tubes are insulating and which metallic in combination with the degree of chirality. The challenge to be met for detailed synchrotron radiation studies is that of obtaining macroscopically ordered samples for study, rather than the ensemble of more or less ordered nanotubes presently available. Nevertheless, there are some interesting results available on the electronic structure.

5.1. XAS/RIXS of carbon nanotubes

Electronic structure studies reported thus far on carbon nanotubes include XAS [76, 77], PES/XPS [77–79], and XES/RIXS [76, 79]. Figure 6 shows XAS data from a sample of relatively uniform single-walled nanotubes produced at Rice University, often denoted 'bucky-paper' [76], which gives a direct impression of this state of affairs. The correspondence to graphite is clear, even down to the excellently resolved σ^* threshold region, and the overall correspondence was enhanced here (compare to figure 4 via the use of 'non-oriented' graphite). It can be shown [77] that a *uniformly distributed ensemble* of carbon nanotubes, with the assumption that the electron structure can be approximated by that of pure graphene in a cylindrical configuration, should give a π^*/σ^* height ratio close to 1. This is in good agreement with the data in figure 6. Some modifications in the intensity ratios can be expected to occur due to symmetry considerations [80] or to the presence of different allotropes, for example, the sp^3-like nanotubes recently suggested [81].

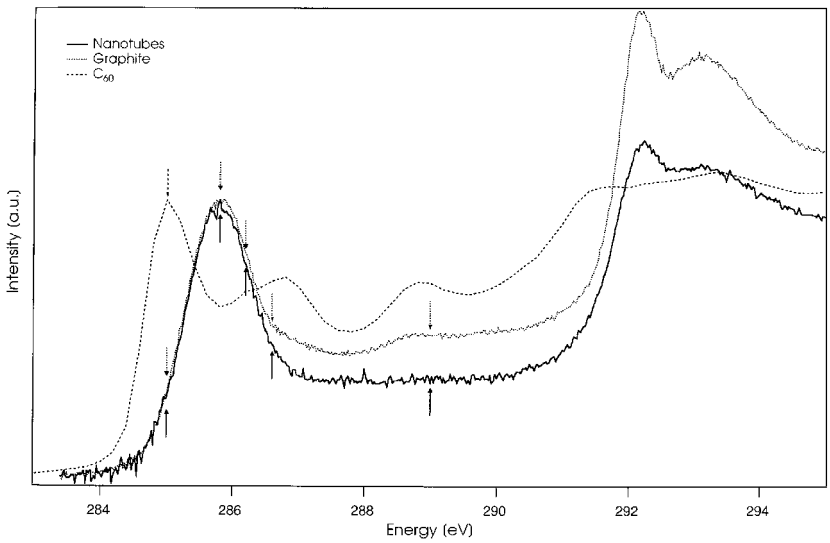

Figure 6. C 1s XAS data of the indicated samples [76].

Perhaps more surprisingly, the RIXS data of [76] are also in good agreement with those of non-oriented graphite. This is naively less expected because the dispersion of peaks in RIXS is, as noted in section 4.3, related to the energy–momentum relationship for electronic states. That relationship is, for a given nanotube, strongly modified due to the quantum confinement in one direction. Nevertheless, the ensemble average of nanotubes displays a dispersion quite similar to the non-oriented graphite. Examining some of the electronic band structures available in the literature for small-diameter nanotubes thought to make up 'bucky-paper' [82–84], one finds that the available vertical transition energies near E_F which define the strongest observed dispersions in RIXS [65, 66, 76] are relatively well preserved in the nanotubes, which would appear to satisfactorily account for the observed trend.

6. C_{60}

C_{60} has icosahedral symmetry, which for the truncated icosahedron means that all 60 atoms are formally equivalent and lie on the surface of a sphere [85]. A spherical model serves to describe the room-temperature solid (often called 'fullerite') as well to a first approximation; synchrotron XRD showed early on that the molecules decorate a cubic lattice whose symmetry is fcc [86], although this is an approximation due to the correlated motions of the molecules [87,88]. Nevertheless, it serves to emphasize that the intermolecular interactions are quite weak, typical of a molecular solid. This is consistent with the observation that the intermolecular and intramolecular vibrations are well separated in energy, with the former localized below 6 meV and the latter between 34 and 196 meV [89].

The icosahedral symmetry entails as well that the spherical harmonics serve as basis functions to a first approximation for the electronic states, with the high degeneracies partially broken for higher angular momenta due to the symmetry lowering imposed by the atomic lattice [90]. This has the consequence that relatively few molecular orbitals account for the 240 valence electrons binding the C_{60} molecule, which has a closed outer shell in the ground state. This shell is five-fold degenerate with h_u symmetry, and is often dubbed the highest occupied

molecular orbital (HOMO). The lowest unoccupied MO (LUMO) is three-fold degenerate with t_{1u} symmetry. These π-like states are expected to be modified in the solid due to translational symmetry and intermolecular coupling of the order of 0.5 eV, but the basic electronic structure of fullerite is expected to strongly resemble that of the molecule. A separate consideration is that changing the population of a given shell, as PES entails, brings with it a cost in terms of correlation energy which a one-electron model does not account for [91]—it can be thought of roughly as a problem of charging a metallic shell with a 7 Å diameter. While this will be reduced in the solid state by dielectric screening, it is still an important ingredient in understanding the electronic structure of fullerene solids and surfaces.

The variability of the interaction of C_{60} with surfaces of other materials, plus the unique and fascinating electronic structure of pure fullerite, have stimulated relatively numerous studies. Since synchrotron studies of the surface structure of C_{60} were not undertaken, I will begin the review of fullerene problems with work on the surface electronic structure, and then move to studies of C_{60} monolayers on surfaces. Much of this work has already been reviewed [92–94], and so I will focus on a few illustrative examples.

6.1. XPS of the surface of solid C_{60} and K_3C_{60}

As for graphite, the surface of fullerite is inert and thus convenient for surface science studies. Typically a (111) surface is exposed, although observation of (100) faces has been reported [95]. XPS studies of fullerite surfaces have generally been performed on multilayer films. A difficulty in these studies has been the occurrence of steady-state charging due to exposure to the light source, which often uniformly shifts all features [96]. This is no barrier to the measurement of absolute binding energies if precautions are taken [7, 97].

Angle-dependent C 1s XPS of such films shows a shift to higher binding energy with increasing emission angle, relative to normal emission [98,99]. This shows that the energy cost of creating a 1s vacancy near the surface is higher than it is further from the surface, consistent with better dielectric screening in the interior of the sample. Initially this was interpreted in terms of ionizing the surface layer molecules, at atoms at or away from the surface, in keeping with the localized nature of the 1s orbital [98]. However, quantum chemical calculations indicate the the screening of a core hole by the valence bands 'depolarizes' the valence charge of the core hole state, and leads to a more or less uniform positive charge distribution over the probe molecule, as one expects for a valence hole [99]. This result is in keeping with the calculated behaviour of extra charges in general on fullerenes. Hence the observed shift of $\sim$0.1 eV had to be interpreted in terms of first and second layer *molecules*, and indeed was consistent with the value of the dielectric constant of about 4.

Recently the (111) surface of annealed K_3C_{60} has been studied quite intensively. This is a prototypical superconductor with a transition temperature T_c near 19 K, confirmed recently by the observation of a gap in PES below T_c [101]. It corresponds for the bulk compound to half-filling of the LUMO-derived band, which was suggested early on in a pioneering synchrotron study [102]. While many groups have claimed or assumed for varying reasons that the electronic structure of the surface of K_3C_{60} is identical to that of the bulk, there was for a long time no clear confirmation of that idea, although serious questions were posed [103, 104]. Instead, for example, relatively novel effects like strong Madelung-potential-induced shifts in the C 1s line were invoked to explain the structure and width of that level [105]. These points and several other observations were possible to reconcile recently with angle-dependent synchrotron data [100]. A fundamental result is summarized in figure 7; there it becomes apparent that there is a strong correlation in lineshape between the HOMO-derived band and the C 1s level, which extends to deeper bands as well. Indeed, much of the valence spectrum

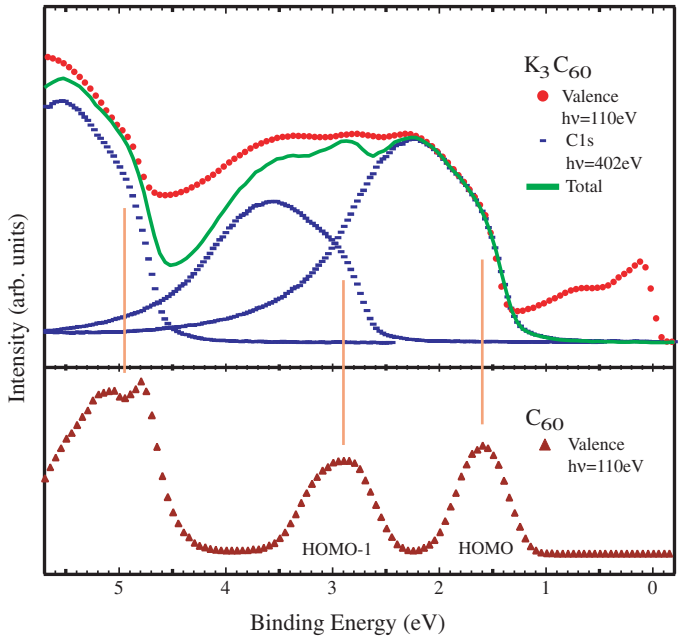

Figure 7. Valence PES data of the indicated samples [100], showing the correlation of the shapes of the deeper valence and C 1s levels. See the text for more details.

(This figure is in colour only in the electronic version)

can be modelled by a sum of C 1s lines, shifted according to the spectral positions for pristine fullerite. The LUMO-derived band, with its markedly different intensity distribution, could also be explained within this model. This can be shown to be due to a rigid band shift of the HOMO and C 1s levels, which was pointed out to be common to all known charge transfer compounds of K and C_{60}. It is reminiscent of the observation noted above for graphite interacting with K. More importantly, the contributions of the bulk and a charge-deficient surface could be separated, and the states at E_F were shown to be largely derived from the bulk of the sample.

6.2. Structural studies of adsorbed C_{60}

There are many observed structures and reconstructions for monolayers and submonolayers of adsorbed C_{60}, which can be roughly catalogued according to bonding type and strength [93]. The large size and electron-scattering cross section of a fullerene molecule entails, however, drawbacks for the determination of the interface structure. Surface sensitive synchrotron XRD has been shown to be a powerful tool for solving this problem.

A relatively well known case is the adsorption of C_{60} on Au(110), which converts the pristine surface (2×1) reconstruction to a (6×5) reconstruction. This was first identified using scanning tunnelling microscopy (STM) [106], which necessitated some guesswork regarding the details of the Au atomic arrangements at the interface. XRD shows instead that two molecular sites must exist, with a height difference corresponding to one Au atomic diameter, and provides details of a more complex underlying Au reconstruction [107]. A substrate reconstruction under a much thicker layer of C_{60} adsorbed on Ge(111)-c(2×8) was also observed using synchrotron XRD [108], in intriguing contrast to the case for C_{60} adsorbed on Si(111)-(7×7) [109].

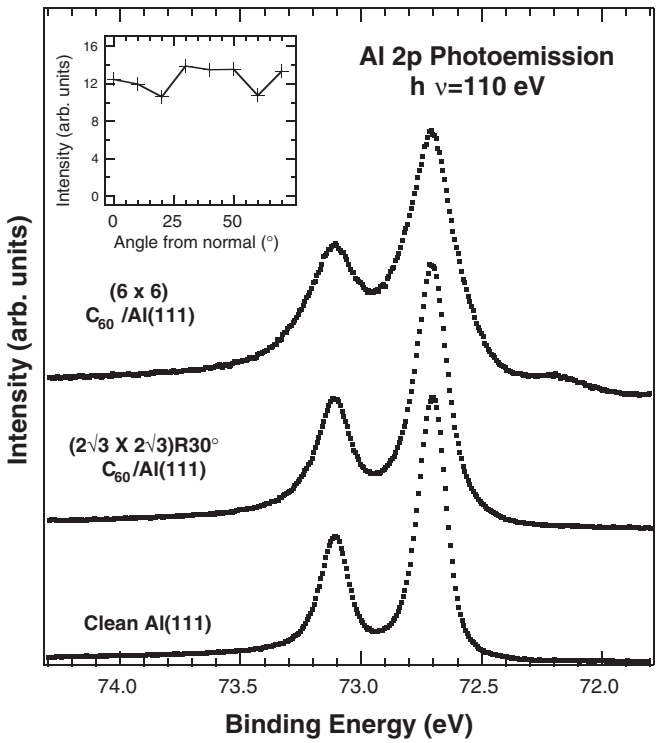

Figure 8. Al 2p PES for C_{60}/Al(111). The increasing spectra width moving upward in the figure gives a measure of the overall hybrization strength, whereas the small peak at 72.7 eV is connected to the reconstructed surface. Inset: angle-dependence of the reconstruction-induced peak at ∼72.2 eV, showing that the ratio of this peak to others is relatively invariant [93], and thus a useful measure of the Al atomic population strongly perturbed in the reconstruction. See the text for more details.

XPS and XAS have also been used to gain information on surface reconstructions associated with C_{60} monolayer adsorption. A particularly interesting case is that of C_{60}/Al(111)-c(6 × 6) [93, 110]. STM shows that the monolayer is reconstructed, with one third of the molecules displaced away from the surface by about 2 Å, and the remaining two thirds arranged in a honeycomb pattern [110]. The high temperature required to achieve this equilibrium structure, combined with the van der Waals separation implied in the measure heights, suggest that the displace molecules must be 'tethered' somehow to the metal surface. The C 1s lines for this system are extremely narrow, however, which is attributed to the covalent nature of the metal-fullerene bonding for this system—for this reason, no structural information is apparent in the profile, presumably once again due to intramolecular screening of the core hole [99]. XPS of the Al 2p level, on the other hand, gives a clear signal of roughly six surface Al atoms being strongly perturbed due to the reconstruction, which are deduced to take part in the surface reconstruction which constitutes the above-mentioned tether (see figure 8). XAS further bolsters the picture of a covalent bond, in that the near-edge features of both π^* and σ^* symmetry are significantly broadened compared to pure C_{60}, and to C_{60} adsorbed on Au(110) [93].

Vibrational properties of adsorbed C_{60} have been studied using synchrotron-based infrared spectroscopy in at least two cases. At the passive H–Si(111), a new vibrational mode was discovered, and attributed tentatively to the lowered symmetry in the monolayer [111]. At

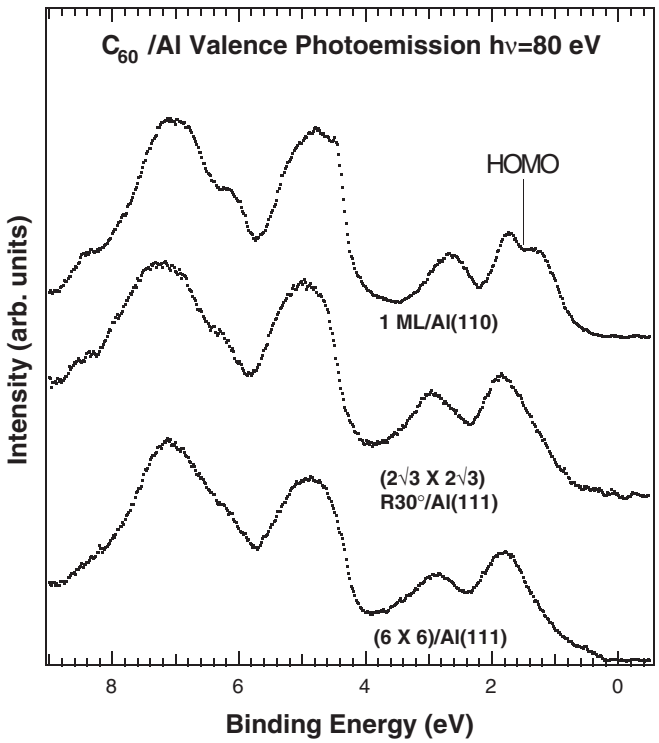

Figure 9. C_{60}-derived valence PES for the indicated samples [93] (an estimated pure-Al background has been subtracted in all cases). The splitting apparent for C_{60} adsorbed on Al is a clear confirmation of covalent bonding for these systems.

the same time, the general similarity to pure C_{60} indicated van der Waals bonding, with slight modifications of the interface indicated by a shifted Si–H stretching frequency. For C_{60} adsorbed on noble metal surfaces, the induced broad-band absorption spectra could be related to microscopic frictional forces, which were interpreted in terms of a significant Fermi-level DOS induced on C_{60} in all cases studied there [2].

6.3. Electronic structure studies of adsorbed C_{60}

Early in the study of C_{60}, it was often assumed that adsorption on metal surfaces could be interpreted in terms of charge transfer from metal to C_{60}. This was quickly found to be an oversimplification [96], and in some cases quite incorrect [93, 110, 112]. Figure 9 shows how this is reflected in the electronic structure of C_{60}/Al(111)-c(6 × 6). The narrow, molecular orbitals of solid C_{60} evolve to an obviously split HOMO line for C_{60}/Al(110), and indicate even stronger interactions for one of the split HOMO bands for the two phases on Al(111) [93], with no significant LUMO-derived intensity characteristic of charge transfer. The high degeneracy of the molecular orbital facilitates this observation. Deeper bands, however, continue to show rigid band shifts relative to one another, including the C 1s line, as illustrated in figure 16 of [93]. XAS can also be interpreted along these lines [93, 113], although the arguments are more complex [7]. Notably, C_{60} adsorption on Si surfaces [114] shares many of the basic properties of C_{60}/Al, albeit with stronger bonding [93].

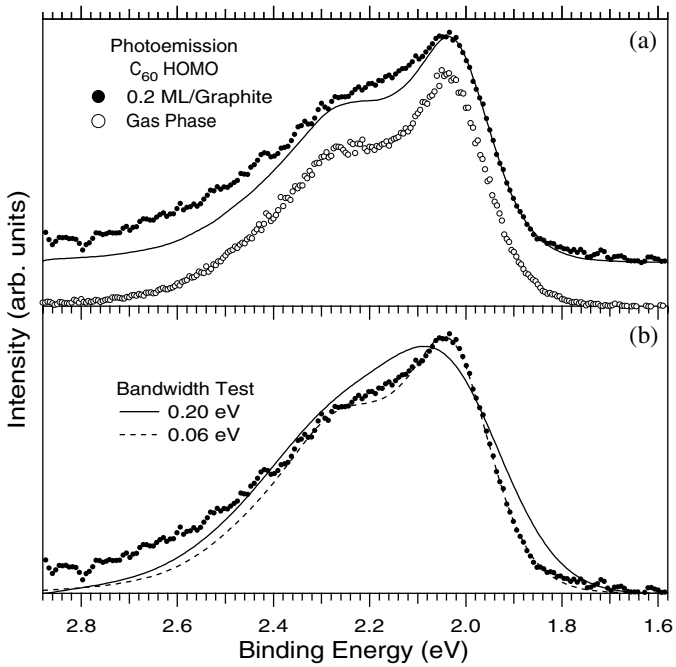

Figure 10. C_{60}-derived valence PES for the indicated samples [115]. The similarity of gas phase to monolayer is apparent in the upper figure, where the smooth curve compared to the monolayer data is the gas phase data broadened to account for the slightly worse resolution. The lower figure shows that very little extra broadening (about 0.2 eV) can be accommodated in the monolayer spectrum compared to the gas phase, giving a semiquantitative measure of the possible dispersion-induced broadening in the data.

6.4. Vibrational coupling to the electronic states of condensed C_{60}

The role of vibrations for the electronic states of condensed C_{60} has been a subject of debate, driven primarily by the difficulty of measuring band dispersions in ARPES [116–120]. Synchrotron studies at low photon energies showed the strongest effects [117, 118, 120], as expected, but without conclusive proof of significant occupied band dispersions. Although the possibility of resolving band dispersions is expected to be reduced due to orientational disorder [121, 122], those state-of-the-art calculations do not describe the available PES data quantitatively; compare, for example, the uppermost curve in figure 6(a) of [122] to the corresponding data shown in the left-hand side of figure 7 of [119] at $k_{\|} \approx 0.655$. On the other hand, a broadened version of the gas phase data [123] compares well to many of the spectra in figure 7 of [119]. This suggests that intramolecular vibrations coupling to the valence hole may indeed play a dominant role in explaining the observed bandwidths in fullerite. This hypothesis obtains strong support from a study of a single layer of C_{60} on graphite, for which the low-temperature spectra even more strongly resemble the gas phase data [115], shown in figure 10. Other effects necessary to take into account when analysing ARPES data of fullerite are the surface screening shift and mean free path effects [115]. Thus, the understanding of the electronic states (at the surface) of fullerite and for an (almost-)isolated two-dimensional layer of C_{60} is far from complete.

7. Summary and outlook

Synchrotron studies of carbon surfaces have given detailed qualitative and quantitative insights into many structural and electronic properties of the samples described. Clearly there are further developments to be awaited on all fronts. Some topics in which the largest gains are yet to come are the carbon nanotubes, for which greater uniformity and order in the samples would repay itself handsomely, in terms of greater resolution and detail beyond what is generally achievable in, for example, a transmission electron microscope. The complex reconstructions for certain adsorbed C_{60} layers would also be an interesting challenge for coming XRD and theoretical efforts. Considering the importance of the metal-to-nanotube contact for future electronics applications, the well studied C_{60}-to-metal contact has surely a storehouse of information to share, if properly exploited; at present there are surely many interesting cases waiting to be characterized experimentally, and very little theoretical work. Vibrational effects are shown to be strong in many aspects of electronic excitations for these systems, and constitute an interesting challenge for theorists and experimentalists alike. Synchrotrons will continue to play an important role in advancing the (materials) science of these systems for the foreseeable future.

Acknowledgments

It is a pleasure to acknowledge my many collaborators and discussion partners on these issues, including A J Maxwell, C Puglia, D Arvanitis, J Schiessling, L Kjeldgaard, T Käämbre, I Marenne, J Schnadt, J N O'Shea, S Andersson, P Rudolf, R Ahuja, O Eriksson, J-E Rubensson, J Nordgren and N Mårtensson. I would also like to thank D T Colbert, K Bobrov and J Nordgren for permission to use figures 1, 2 and 6 respectively. This work was funded in part by Vetenskapsrådet and the CARAMEL Consortium, which was funded by Stiftelsen för Strategisk Forskning.

References

[1] Dresselhaus M S, Dresselhaus G and Eklund P C 1996 *Science of Fullerenes and Carbon Nanotubes* (New York: Academic) ch 2
[2] Dumas P *et al* 1999 *Surf. Sci.* **433–5** 797
[3] Hüfner S 1996 *Photoelectron Spectroscopy* (Berlin: Springer) p 193
[4] Mårtensson N and Nilsson A 1995 *Applications of Synchrotron Radiation (Springer Series in Surface Sciences vol 35)* ed W Eberhardt (Berlin: Springer) ch 3
[5] Kevan S D 1992 *Angle-Resolved Photoemission* (Amsterdam: Elsevier)
[6] Eberhardt W 1995 *Applications of Synchrotron Radiation (Springer Series in Surface Sciences vol 35)* ed W Eberhardt (Berlin: Springer) ch 6
[7] Brühwiler P A, Karis O and Mårtensson N at press
[8] Stöhr J 1992 *NEXAFS Spectroscopy* (Berlin: Springer)
[9] Schnadt J *et al* 2001 *Nucl. Instrum. Methods* B **184** 609
[10] Guo J, Skytt P, Wassdahl N and Nordgren J 2000 *J. Electron Spectrosc. Related Phenom.* **110–11** 41
[11] Gel'mukhanov F and Ågren H 1999 *Phys. Rep.* **312** 87 and references therein
[12] Shirley E L 2000 *J. Electron Spectrosc. Related Phenom.* **110–11** 305
[13] Kotani A and Shin S 2001 *Rev. Mod. Phys.* **73** 203
[14] Diederich L, Küttel O M, Aebi P and Schlapbach L 1998 *Surf. Sci.* **418** 219
[15] Hollman P, Björkman H, Alahelisten A and Hogmark S 1998 *Surf. Coat. Tech.* **105** 169
[16] Mercer T W, Russel J J N and Pehrsson P E 1997 *Surf. Sci.* **392** L21
[17] Küttel O M *et al* 1995 *Surf. Sci.* **337** L812
[18] Thoms D E and Butler J E 1995 *Surf. Sci.* **328** 291
[19] Himpsel F J, Knapp J A, van Vechten J A and Eastman D E 1979 *Phys. Rev.* B **20** 624

[20] Morar J F *et al* 1985 *Phys. Rev. Lett.* **54** 1960
[21] Graupner R, Ristein J, Ley L and Jung C 1999 *Phys. Rev.* B **60** 17 023
[22] Bobrov K *et al* 2001 *Phys. Rev.* B **63** 165421
[23] Hoffman A *et al* 1998 *Appl. Phys. Lett.* **73** 1152
[24] Morar J F *et al* 1986 *Phys. Rev.* B **33** 1340
[25] Pandey K 1982 *Phys. Rev.* B **25** 4338
[26] Graupner R *et al* 1997 *Phys. Rev.* B **55** 10 841
[27] Morar J F *et al* 1986 *Phys. Rev.* B **33** 1346
[28] Carson R D and Schnatterly S E 1987 *Phys. Rev. Lett.* **59** 319
[29] Hoffman A *et al* 1999 *Phys. Rev.* B **59** 3203
[30] Shirley E L 1998 *Phys. Rev. Lett.* **80** 794
[31] Mauri F and Car R 1995 *Phys. Rev. Lett.* **75** 3166
[32] Charlier J-C, Gonze X and Michenaud J-P 1994 *Europhys. Lett.* **28** 403
[33] Schabel M C and Martins J L 1992 *Phys. Rev.* B **46** 7185
[34] Strocov V N *et al* 2001 *Phys. Rev.* B **64** 075105
[35] Shirley E L, Terminello L J, Santoni A and Himpsel F J 1995 *Phys. Rev.* B **51** 13 614
[36] Law A R, Johnson M T and Hughes H P 1986 *Phys. Rev.* B **34** 4289
[37] van Attekum P M T M and Wertheim G K 1979 *Phys. Rev. Lett.* **43** 1896
[38] Sette F *et al* 1990 *Phys. Rev.* B **41** 9766
[39] Bennich P *et al* 1999 *Phys. Rev.* B **59** 8292
[40] Prince K C *et al* 2000 *Phys. Rev.* B **62** 6866
[41] Balasubramanian T, Andersen J N and Walldén L 2001 *Phys. Rev.* B **64** 205420
[42] See, e.g., Hüfner S 1996 *Photoelectron Spectroscopy* (Berlin: Springer) p 122
[43] Mele E J and Ritsko J J 1979 *Phys. Rev. Lett.* **43** 68
[44] Chen C T and Sette F 1989 *Rev. Sci. Instrum.* **60** 1616
[45] Willis R F, Feuerbacher B and Fitton B 1971 *Phys. Rev.* B **4** 2441
[46] Bianconi A, Hagström S B M and Bachkrach R Z 1977 *Phys. Rev.* B **16** 5543
[47] Marchand D *et al* 1984 *Phys. Rev.* B **30** 4788
[48] Eberhardt W, McGovern I T, Plummer E W and Fisher J E 1980 *Phys. Rev. Lett.* **44** 200
[49] Heske C *et al* 1999 *Phys. Rev.* B **59** 4680
[50] Shirley E L 1998 *Phys. Rev.* B **58** 9579
[51] Schönhense G, Westphal C, Bansmann J and Getzlaff M 1992 *Europhys. Lett.* **17** 727
[52] Brühwiler P A *et al* 1995 *Phys. Rev. Lett.* **74** 614
[53] Ahuja R *et al* 1996 *Phys. Rev.* B **54** 14 396
[54] van Veenendal M and Carra P 1997 *Phys. Rev. Lett.* **78** 2839
[55] Sandell A *et al* 1997 *Phys. Rev. Lett.* **78** 4994
[56] Ma Y *et al* 1993 *Phys. Rev. Lett.* **71** 3725
[57] Kempgens B *et al* 1997 *Phys. Rev. Lett.* **79** 3617
[58] Köppel H *et al* 1997 *J. Chem. Phys.* **106** 4415
[59] Myrseth V *et al* unpublished
[60] Ma Y *et al* 1989 *Phys. Rev. Lett.* **63** 2044
[61] Ruffieux P *et al* 2001 *Phys. Rev. Lett.* **84** 4910
[62] Eisebitt S and Eberhardt W 2000 *J. Electron Spectrosc. Relat. Phenom.* **110–11** 335
[63] Minami T and Nasu K 1998 *Phys. Rev.* B **57** 12 084
[64] Brühwiler P A *et al* 1996 *Phys. Rev. Lett.* **76** 1761
[65] Carlisle J A *et al* 1995 *Phys. Rev. Lett.* **74** 1234
[66] Carlisle J A *et al* 2000 *J. Electron Spectrosc. Relat. Phenom.* **110–11** 323
[67] Li Z Y, Hock K M and Palmer R E 1991 *Phys. Rev. Lett.* **67** 1562
[68] See, e.g., Dresselhaus M S, Dresselhaus G and Eklund P C 1996 *Science of Fullerenes and Carbon Nanotubes* (New York: Academic) ch 19
[69] Lemay S G *et al* 2001 *Nature* **412** 617
[70] Drotar J T *et al* 2001 *Phys. Rev.* B **64** 125417
[71] Maniwa Y *et al* 2001 *Phys. Rev.* B **64** 073105
[72] Kiang C-H *et al* 1998 *Phys. Rev. Lett.* **81** 1869
[73] Thess A *et al* 1996 *Science* **273** 483
[74] Henrard L, Loiseau A, Journet C and Bernier P 2000 *Eur. J. Phys.* B **13** 661
[75] Ouyang M, Huang J-L, Cheung C L and Lieber C M 2001 *Science* **292** 702
[76] Eisebitt S *et al* 1998 *Appl. Phys.* A **67** 89

[77] Schiessling J *et al* unpublished
[78] Ago H *et al* 1999 *J. Phys. Chem.* B **103** 8116
[79] Bulusheva L G *et al* 2001 *J. Phys. Chem.* B **105** 4853
[80] Kleiner A and Eggert S 2001 *Phys. Rev.* B **64** 113402
[81] Stojkovic D, Zhang P and Crespi V H 2001 *Phys. Rev. Lett.* **87** 125502
[82] Hamada N, Sawada S-I and Oshiyama A 1992 *Phys. Rev. Lett.* **68** 1579
[83] Charlier J-C and Issi J-P 1998 *Appl. Phys.* A **67** 79
[84] Mintmire J W and White C T 1998 *Appl. Phys.* A **67** 65
[85] See, e.g., Dresselhaus M S, Dresselhaus G and Eklund P C 1996 *Science of Fullerenes and Carbon Nanotubes* (New York: Academic) ch 4
[86] Heiney P A *et al* 1991 *Phys. Rev. Lett.* **66** 2911
[87] Chow P C *et al* 1992 *Phys. Rev. Lett.* **69** 2943
[88] See, e.g., Dresselhaus M S, Dresselhaus G and Eklund P C 1996 *Science of Fullerenes and Carbon Nanotubes* (New York: Academic) ch 7
[89] See, e.g., Dresselhaus M S, Dresselhaus G and Eklund P C 1996 *Science of Fullerenes and Carbon Nanotubes* (New York: Academic) ch 11
[90] See, e.g., Dresselhaus M S, Dresselhaus G and Eklund P C 1996 *Science of Fullerenes and Carbon Nanotubes* (New York: Academic) ch 12
[91] Lof R W *et al* 1992 *Phys. Rev. Lett.* **68** 3924
[92] Rudolf P 1996 *Fullerenes and Fullerene Nanostructures* ed H Kuzmany, J Fink, M Mehring and S Roth (Singapore: World Scientific) p 263
[93] Maxwell A J *et al* 1998 *Phys. Rev.* B **57** 7312
[94] Rudolf P, Golden M S and Brühwiler P A 1999 *J. Electron Spectrosc. Relat. Phenom.* **100** 409
[95] Wang X-D *et al* 1993 *Phys. Rev.* B **47** 15 923
[96] Maxwell A J *et al* 1994 *Phys. Rev.* B **49** 10 717
[97] Maxwell A J *et al* 1996 *Chem. Phys. Lett.* **260** 71
[98] Gensterblum G *et al* 1994 *Phys. Rev.* B **50** 11 981
[99] Rotenberg E *et al* 1996 *Phys. Rev.* B **54** R5279
[100] Schiessling J *et al* unpublished
[101] Hesper R, Tjeng L H, Heeres A and Sawatzky G A 2000 *Phys. Rev. Lett.* **85** 1970
[102] Chen C T *et al* 1991 *Nature* **352** 603
[103] Wertheim G K and Buchanan D N E 1993 *Phys. Rev.* B **47** 12 912
[104] Hesper R, Tjeng L H, Heeres A and Sawatzky G A 2000 *Phys. Rev.* B **62** 160461
[105] Goldoni A *et al* 1999 *Phys. Rev.* B **59** 16 071
[106] Gimzewski J K, Modesti S and Schlittler R R 1994 *Phys. Rev. Lett.* **72** 1036
[107] Pedio M *et al* 2000 *Phys. Rev. Lett.* **85** 1040
[108] Kidd T *et al* 1998 *Surf. Sci.* **397** 185
[109] Hong H *et al* 1992 *Appl. Phys. Lett.* **61** 3127
[110] Maxwell A J *et al* 1995 *Phys. Rev.* B **52** R5546
[111] Dumas P *et al* 1996 *Surf. Sci.* **368** 330
[112] Hunt M R C, Modesti S, Rudolf P and Palmer R E 1995 *Phys. Rev.* B **51** 10 039
[113] Maxwell A J *et al* 1997 *Phys. Rev. Lett.* **79** 1567
[114] Sakamoto K *et al* 1999 *Phys. Rev.* B **60** 2579
[115] Brühwiler P A *et al* 1997 *Chem. Phys. Lett.* **279** 85
[116] Wu J *et al* 1992 *Physica* C **197** 251
[117] Gensterblum G *et al* 1993 *Phys. Rev.* B **48** 14 756
[118] Benning P J, Olson C G, Lynch D W and Weaver J H 1994 *Phys. Rev.* B **50** 11 239
[119] Golden M S *et al* 1995 *J. Phys.: Condens. Matter* **7** 8219
[120] Gensterblum G 1996 *J. Electron Spectrosc. Related Phenom.* **81** 89
[121] Shirley E L and Louie S G 1993 *Phys. Rev. Lett.* **71** 133
[122] Louie S G and Shirley E L 1993 *J. Phys. Chem. Solids* **54** 1767
[123] Lichtenberger D L *et al* 1991 *Mat. Res. Soc. Symp. Proc.* **206** 673